Journal of Alloys and Compounds 502 (2010) 24–27

Contents lists available at ScienceDirect

Journal of Alloys and Compounds

journal homepage: www.elsevier.com/locate/jallcom

Optical properties of ZnO/PMMA nanocomposite films

B. Kulyk[a,*], V. Kapustianyk[a], V. Tsybulskyy[a], O. Krupka[b], B. Sahraoui[c]

[a] Department of Physics, Scientific and Educational Center "Fractal", Scientific-Technical and Educational Center of Low Temperature Studies, Ivan Franko National University of L'viv, 50 Dragomanova Str., L'viv, Ukraine
[b] Department of Chemistry, Kyiv Taras Shevchenko National University, 60 Volodymyrska Str., Kyiv, Ukraine
[c] Institute of sciences and molecular technologies of Angers, MOLTECH Anjou - UMR CNRS 6200, Molecular interaction nonlinear optics and structuring MINOS, 2 bd Lavoisier, 49045 Angers Cedex 2, France

ARTICLE INFO

Article history:
Received 6 February 2010
Received in revised form 14 April 2010
Accepted 23 April 2010
Available online 4 May 2010

Keywords:
ZnO nanocrystals
PMMA
Photoluminescence
Varshni formula

ABSTRACT

The ZnO nanocrystals (ZnO NCs) with particle size, less than 100 nm, have been blended with polymethylmethacrylate (PMMA) by solution mixing to prepare PMMA/ZnO nanocomposite films. The structure of ZnO/PMMA nanocomposite films was characterized using X-ray diffractometry. The prepared nanocomposite films are highly transparent and a clear excitonic peak is observed in their absorption spectra. Measurements of temperature evolution of the photoluminescence (PL) spectra show intensive UV emission peak corresponding to the donor-bound excitons with binding energy of 51 meV and green emission band related to the intrinsic defects in ZnO. The temperature evolution of the emission peaks energy position, intensity and integral intensity in ZnO/PMMA nanocomposite films were examined.

1. Introduction

Semiconductor nanoparticles are receiving much attention owing to their novel physical and chemical properties. In comparison with the bulk semiconductor they possess many specific properties such as ultrafast optical nonlinear response, photoelectricity switch and attractive piezoelectric properties. The recent high-speed development of biotechnology, energy sources, environment and advanced manufacture technology urgently require considerable material miniaturization, high integration and high-density transmission, which imply a broad application for semiconductor nanoparticles.

It is expected that ZnO nanoparticles should possess the characteristics close to those for the bulk zinc oxide. First of all this concerns a large exciton binding energy (nearly 60 meV) and excellent stability. At the same time, ZnO nanoparticles have attracted much attention due to the strong commercial desire for photocatalysis, photoelectrochemistry, blue and UV light emitters [1] and detectors based on their specific properties. Indeed, it is well known that small particles have the large surface-to-volume ratio that strongly modifies the physical processes in the nanocomposites. The PL spectra of the ZnO nanoparticle samples usually show a nearband-edge (NBE) UV line accompanied by a strong visible luminescence, which can result in decrease of the carrier/exciton lifetime and higher emission efficiency of the UV light emitting devices. Therefore, the most crucial aspects of high luminescence efficiencies from ZnO nanoparticles are the surface texture and an efficient surface passivation. Fortunately, polymer capping can effectively passivate the surface of nanoparticles and reduce the surface-related visible emission [2,3].

Generally, the UV emission is attributed to the exciton radiative recombination while that of the visible emission still remains uncertain. Various mechanisms have been proposed, in fact, most probable origin of the visible PL is caused by the intrinsic defects. The density of these defects has to be higher on the surface of the sample, first of all due to the zinc and oxygen vacancies. In the case of nanoparticles the influence of surface is expected to be more pronounced due to the increased surface-to-volume ratio.

In this paper we report the method of ZnO/PMMA nanocomposite film preparation as well as the investigation of optical absorption and temperature evolution of PL in order to compare the features of ZnO/PMMA composite film with the bulk ZnO.

2. Experimental details

The investigated samples were manufactured on the basis of ZnO nanocrystals embedded into PMMA polymeric matrix. For preparation of the nanocomposite films the nanopowder from Sigma–Aldrich (<100 nm in size) have been used. The glass substrates used were carefully cleaned in a commercial surfactant using ultrasonication. The cleaning procedure was ended by baking in a 200 °C oven for 60 min. Spin coating technique was used to fabricate nanocomposite films with ZnO nanocrystals dispersed in PMMA. The solution of 1,2,2-trichloroethane containing PMMA 100 g/L and ZnO was coated on BK7 glass slides. The weight concentration of ZnO nanocrystals in PMMA were 5, 10 and 15%. The principle of deposition (of the mixture with certain viscosity) is based on a homogeneous spreading out of the solution on the

* Corresponding author. Tel.: +380 509128436.
E-mail address: bohdan_kulyk@yahoo.com (B. Kulyk).

0925-8388/$ – see front matter © 2010 Elsevier B.V. All rights reserved.
doi:10.1016/j.jallcom.2010.04.162

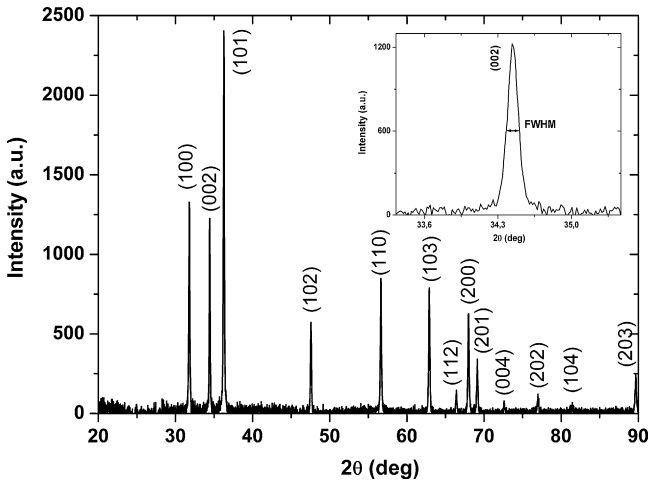

Fig. 1. X-ray diffraction pattern of ZnO/PMMA (15 wt.% of ZnO NCs) nanocomposite film. In inset – the FWHM of (0 0 2) diffraction peak.

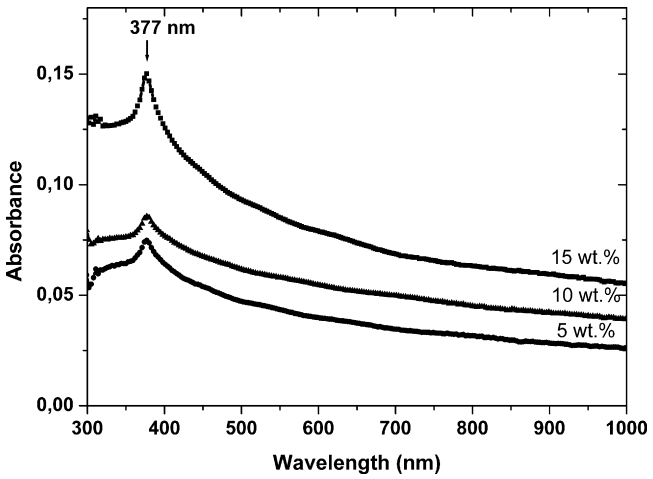

Fig. 2. UV–vis spectra of ZnO/PMMA nanocomposite films with different ZnO NCs concentrations: 5, 10, and 15 wt.%. The thickness of all films is around 1 μm.

rotating substrate with an angular speed of 1000 rpm during 60 s. Immediately after the deposition, the thin films were cured in an 60 °C oven for 60 min in order to eliminate any remaining solvent. The thickness of nanocomposite films was verified by a Dektak surface stylus profiler (Veeco) to be about 1 μm.

The XRD measurements were carried out using STOE STADI P diffractometer with linear position sensitive detector in transmission Bragg–Brentano geometry (Cu $K\alpha_1$ radiation, Ge(1 1 1) monochromator, 2θ range: 20–90°, step – 270 s).

The optical absorption spectra in visible and near-UV region were measured using a Lambda 19 spectrometer from PerkinElmer. The temperature evolution of the PL spectra near the intrinsic absorption edge and in a visible region was studied under excitation with a LGI-21 nitrogen laser at 337 nm emission wavelength with 10 ns pulse duration and the power of 1 kW.

3. Results and discussion

3.1. XRD data analysis

Fig. 1 shows X-ray diffraction pattern of the ZnO/PMMA (15 wt.% of ZnO NCs) nanocomposite film. The observed set of sharp diffraction peaks corresponds to the hexagonal wurtzite structure of ZnO. Detailed description of the observed diffraction peaks, their angular position and relative intensity towards most intensive (1 0 1) peak are given in Table 1. Intensive and sharp diffraction peaks of XRD pattern in ZnO/PMMA nanocomposite film are similar to that in ZnO bulk. This confirms that we deal with the nanoparticles of quite large sizes as compared with ZnO quantum dots. The large amount of diffraction peaks corresponding to various crystalline orientations indicates that ZnO NCs within PMMA are disordered and do not have preferred axis orientation.

Table 1
Angular position and relative intensity of the diffraction peaks in XRD pattern of ZnO/PMMA (15 wt.% of ZnO NCs) nanocomposite film.

Diffraction peak	Peak position 2θ (°)	Peak intensity (%)
(1 0 0)	31.79	55.2
(0 0 2)	34.44	51.0
(1 0 1)	36.27	100
(1 0 2)	47.57	23.8
(1 1 0)	56.62	35.4
(1 0 3)	62.91	32.8
(2 0 0)	66.43	6.1
(1 1 2)	68.00	26.2
(2 0 1)	69.13	14.2
(0 0 4)	72.62	3.3
(2 0 2)	77.01	5.0
(1 0 4)	81.45	2.9
(2 0 3)	89.67	10.3

The average size of the particles can be calculated by the Debye–Scherrer formula, i.e.:

$$D = \frac{0.9\lambda}{B\ \cos\theta_B}, \quad (1)$$

where D is the average size of the particle, λ is the X-ray wavelength (1.54 Å), B is the FWHM width of the diffraction peak, and θ_B is the corresponding diffraction angle of the diffraction peak. According to the data presented in Fig. 1 the average particle size of the ZnO nanocrystals calculated on the basis of Eq. (1) for the (0 0 2), (1 0 1) and (1 0 0) diffraction peaks was found to be about 60–65 nm.

3.2. Optical absorption measurements

The absorption spectra of ZnO/PMMA nanocomposite films shown in Fig. 2 clearly demonstrate the absorption peaks at 377 nm (3.29 eV) corresponding to the exciton state in the bulk ZnO [4]. Since the size of ZnO NCs is nearly 100 nm that is much more than the exciton Bohr radius in ZnO (a_B = 2.34 nm [5]) we do not observe in our NCs system any shift of the corresponding peak as manifestation of the quantum confinement effect. The intensity of the peaks enhances with increasing of ZnO NCs concentration.

3.3. PL spectra temperature evolution

Fig. 3 shows the temperature evolution of PL spectra in ZnO nanocrystals embedded into polymeric matrix PMMA in the temperature range from 85 to 290 K. Analysis of the low-temperature PL in ZnO NCs and its comparison with PL in bulk ZnO permits to define the nature and characteristics of the recombination processes in the nanoscale ZnO crystals near the absorption edge. The PL spectra are characterized by intensive emission in the near-UV region and lower emission in the green region of spectrum (507 nm) connected with the presence of intrinsic defects [6,7]. The recombination processes in ZnO NCs differ from that in bulk ZnO mainly, because of the larger surface-to-volume ratio and, therefore, larger amount of defects on the surface. Basing on the previous investigation of PL in NCs [8], the obtained experimental results assume that the UV PL in ZnO NCs in the temperature range of 85–290 K emerges in consequence of recombination of donor-bound excitons (D,X). The maximum of UV peak emission correspond to 382 (3.25 eV) nm at room temperature and its intensity grows with temperature decreasing meanwhile it shifts to shorter wavelength.

The UV emission band from the side of lower energy has the step-like shape with the clearly defined equidistant peaks. Energy

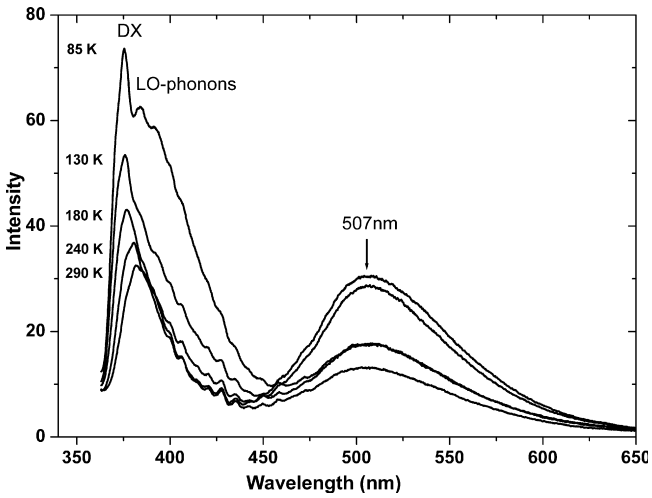

Fig. 3. PL spectra of ZnO NCs embedded into PMMA matrix at 15 wt.% obtained in temperature range of 85–290 K.

distant between these peak is approximately equal to 70 meV, which corresponds to the energy of LO-phonon in ZnO [9,10]. The presence of the LO-phonon peaks define a large exciton–phonon interaction in ZnO NCs, which enhances with temperature decreasing and appears in temperature broadening of UV emission band.

The temperature evolution of green emission band in ZnO NCs is shown in Fig. 4. Increasing of the full integral intensity of the band at cooling is observed due to the suppression of quenching mechanism – thermal activation of nonemitting centers and charge carrier recombination on localised center [11]. The energy position of the band does not depend on temperature in the investigated range. At the same time it is necessary to mention the peculiar temperature dependence of this band intensity with the clear maximum at 210 K, which is not inherent for ZnO. Such a behavior can be attributed to the temperature dependant properties of PMMA, first of all with nonlinear behavior of its electret field. As it is known from the thermally stimulated discharge data in PMMA at the 220–230 K the relaxation processes causing a partial orientational relaxation of dipoles take place. The dipoles of the polar ester side groups ($-COOCH_3$) reorient by local motion around the C–C bond [12,13]. The nature of the "green" band is connected with the deep centers of emission caused by zinc V_{Zn} [14,15] and oxygen vacancies V_O [16,17] and interstitial atoms of zinc (Zn_i) [18].

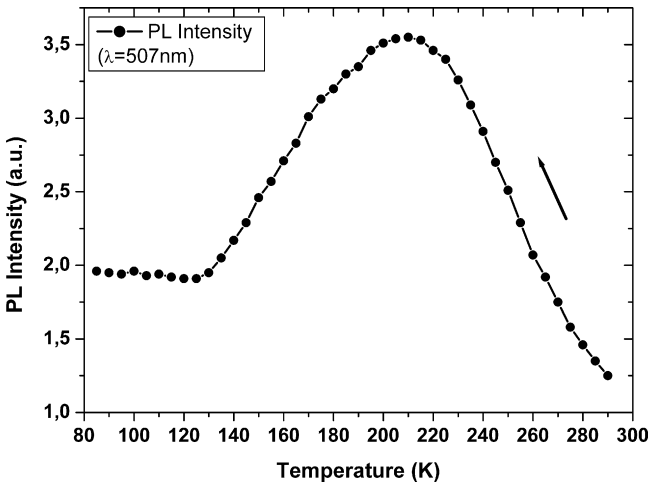

Fig. 4. Temperature evolution of green emission band at 507 nm in ZnO NCs.

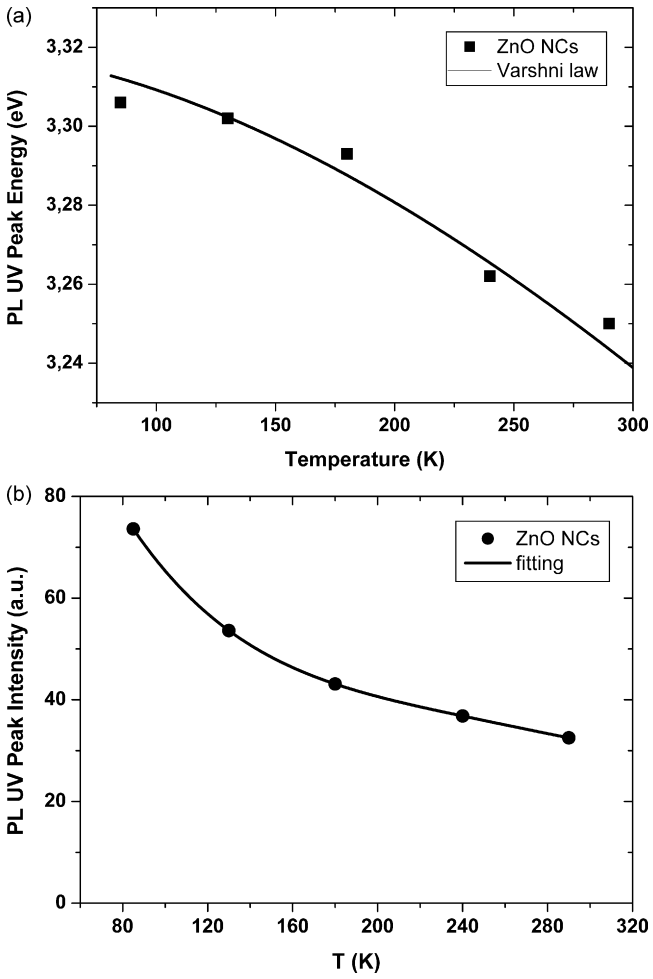

Fig. 5. (a) Energy position with approximation by Varshni law, and (b) intensity of donor-bound exciton emission peak as a function of temperature.

In bulk ZnO the UV emission peak corresponding to the recombination of the free excitons was found to be at higher energy (about 3.3 eV at 300 K) in comparison with ZnO NCs, where UV PL is caused by recombination of bound excitons. The difference in 51 meV between bound exciton peak in ZnO NCs and free exciton peak in ZnO bulk is close to the bound exciton binding energy – 50 meV [19–22].

In Fig. 5 the UV emission peak energy position and its intensity are given depending on temperature. It can be seen that the emission intensity of donor-bound excitons and their energy position diminish with heating. Depending on the temperature, the donor-bound exciton localization energy is 50–60 meV in comparison with free exciton energy in bulk ZnO [8].

Significant diminution of the donor-bound exciton energy with temperature should be related to the presence of different kind of donors in ZnO NCs, for example, oxygen vacancies, interstitial zinc atoms. The width of UV peak also depends on the concentration of the oxygen vacancies responsible for a set of donor levels. Their energy should be different for the bulk of nanoparticle and its surface.

In Fig. 5(a) the temperature dependence of the excitonic peak energy position was approximated by semiempirical formula of Varshni [23]:

$$E(T) = E(0) - \frac{\alpha T^2}{T + \theta_D}, \quad (2)$$

Table 2
Parameters of Varshni formula for the donor-bound excitons in single crystals and nanocrystals of ZnO.

	$E(0)$ (eV)	α (meV/K)
ZnO bulk [7]	3.36	0.67
ZnO NCs	3.32	1.1

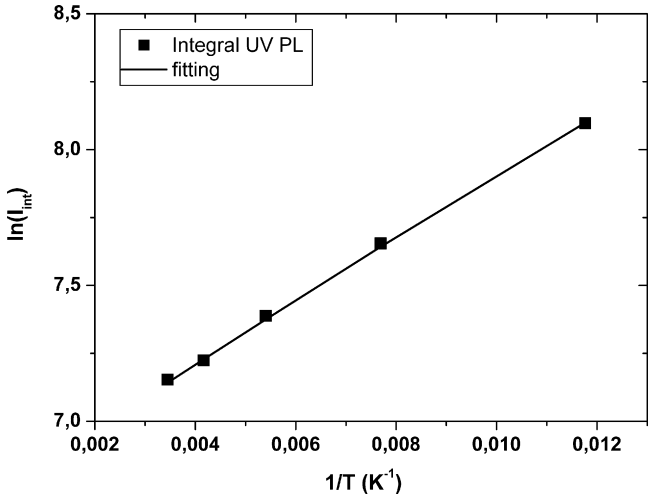

Fig. 6. Log plot of the integral UV PL intensity as a function of the inverse temperature (from 290 to 85 K). Solid line gives linear fitting.

where $E(0)$ is energy at $T = 0$ K, α – parameter, θ_D – Debye temperature.

Table 2 presents the parameters obtained from approximation by Eq. (2), where $\theta_D = 920$ K for the recombination processes [24]. The calculated values of $E(0)$ and parameter α for the UV peak correlate well with the values obtained for single crystals and thin films of ZnO [8,22,25].

The integral intensity of UV emission of PL decreases with temperature increasing due to the effect of thermal quenching and is described by expression [26]:

$$I(T) = \frac{I_0}{1 + A\ \exp(-(E_a/k_B))}, \quad (3)$$

where I_0 is the integral intensity at $T = 0$ K, A is the constant, E_a is the activation energy in the process of thermal quenching, k_B is the Boltzmann constant. Eq. (3) clarifies influence of binding energy of exciton on the emission intensity of PL, which grows almost exponentially with increase of binding energy at permanent temperature. Fig. 6 depicts the dependence of the integral PL intensity of UV band in logarithmic scale on the inverse temperature is shown. The solid line corresponds to fitting of results and possesses a linear character in the investigated temperature region.

4. Conclusions

In the present work, the high-quality ZnO/PMMA nanocomposite films were prepared by embedding of ZnO NCs into PMMA polymeric matrix. The films show high optical transmittance in near-UV–vis region and presence of the near-band excitonic peak. The temperature study of PL in ZnO/PMMA nanocomposite films demonstrates the intensive UV emission, which was connected with donor-bound excitons and lower green emission due to the presence of internal intrinsic defects. When the ZnO structure changes from single crystal to the nanostructures (nanorods, nanotubes, etc.) and then to the nanocomposite film the intensity of UV exciton related band enhance in respect to the intensity of the green band and its energy position could be changed due to the variation of the localised excitonic states corresponding to the different kinds of defects in these three types of materials. The unusual behavior of green band temperature dependence was explained by nonlinear properties of electret field in PMMA caused by reorientation of dipoles within PMMA polymer. Besides, the temperature characteristics of UV band were studied, the binding energy of donor-bound excitons was found to be 51 meV at 290 K.

Acknowledgments

The XRD measurements were performed in “Interdepartmental scientific-educational laboratory of XRD analysis” of Ivan Franko National University of L’viv.

References

[1] A. Chiappini, C. Armellini, A. Chiasera, M. Ferrari, R. Guider, Y. Jestin, L. Minati, E. Moser, G. Nunzi Conti, S. Pelli, R. Retoux, G.C. Righini, G. Speranza, J. Non-Cryst. Solids 355 (2009) 1132–1135.
[2] C.L. Yang, J.N. Wang, W.K. Ge, L. Guo, S.H. Yang, D.Z. Shen, J. Appl. Phys. 90 (2001) 4489.
[3] Y.H. Tong, Y.C. Liu, S.X. Lu, L. Dong, S.J. Cheng, Z.Y. Xiao, J. Sol–Gel Sci. Technol. 30 (2004) 157–161.
[4] Ü. Özgür, Ya.I. Alivov, C. Liu, A. Teke, M.A. Reshchikov, S. Doğan, V. Avrutin, S.-J. Cho, H. Morkoç, J. Appl. Phys. 98 (2005) 1–103.
[5] K.F. Lin, H.M. Cheng, H.C. Hsu, L.J. Lin, W.F. Hsieh, Chem. Phys. Lett. 409 (2005) 208–211.
[6] B.K. Meyer, H. Alves, D.M. Hofmann, W. Kriegseis, D. Forster, F. Bertram, J. Christen, A. Hoffmann, M. Strassburg, M. Dworzak, U. Haboeck, A.V. Rodina, Phys. Status Solidi B 241 (2004) 231.
[7] S. Cho, J. Korean Phys. Soc. 49 (3) (2006) 985–988.
[8] V.A. Fonoberov, K.A. Alim, A.A. Balandin, F. Xiu, J. Liu, Phys. Rev. B 73 (2006) 165317.
[9] J.M. Calleja, M. Cardona, Phys. Rev. B 16 (1977) 3753–3761.
[10] K.A. Alim, V.A. Fonoberov, A.A. Balandin, Appl. Phys. Lett. 86 (2005) 053103.
[11] Q. Li, S.J. Xu, M.H. Xie, S.Y. Tong, Europhys. Lett. 71 (2005) 994–1000.
[12] K. Mazur, J. Phys. D: Appl. Phys. 30 (1997) 1383–1398.
[13] U. Kubon, R. Schilling, J.H. Wendorff, Colloid Polym. Sci. 266 (1988) 123–131.
[14] A.F. Kohan, G. Ceder, D. Morgan, C.G. Van de Walle, Phys. Rev. B 61 (2000) 15019–15027.
[15] B. Guo, Z.R. Qiu, K.S. Wong, Appl. Phys. Lett. 82 (14) (2003) 2290–2292.
[16] S.A. Studenikin, N. Golego, M. Cocivera, J. Appl. Phys. 84 (4) (1998) 2287–2294.
[17] F.H. Leiter, H.R. Alves, A. Hofstaetter, D.M. Hoffmann, B.K. Meyer, Phys. Status Solidi (b) 226 (1) (2001) R4–R5.
[18] N.O. Korsunska, L.V. Borkovska, B.M. Bulakh, L.Yu. Khomenkova, V.I. Kushnirenko, I.V. Markevich, J. Lumin. 102–103 (2003) 733–736.
[19] X.T. Zhang, Y.C. Liu, Z.Z. Zhi, J.Y. Zhang, Y.M. Lu, D.Z. Shen, W. Xu, X.W. Fan, X.G. Kong, J. Lumin. 99 (2002) 149.
[20] J. Chen, T. Fujita, Jpn. J. Appl. Phys. Part 2 41 (2002) L203.
[21] C.R. Gorla, N.W. Emanetoglu, S. Liang, W.E. Mayo, Y. Lu, M. Wraback, H. Shen, J. Appl. Phys. 85 (1999) 2595.
[22] H.J. Ko, Y.F. Chen, Z. Zhu, T. Yao, I. Kobayashi, H. Uchiki, Appl. Phys. Lett. 76 (2000) 1905.
[23] Y.P. Varshni, Physica (Amsterdam) 34 (1967) 149.
[24] A.R. Hutson, J. Phys. Chem. Solids 8 (1959) 467.
[25] S. Loughin, R.H. French, W.Y. Ching, Y.N. Xu, G.A. Slack, Appl. Phys. Lett. 63 (1993) 1182.
[26] D.S. Jiang, H. Jung, K. Ploog, J. Appl. Phys. 64 (1988) 1371.